NUCL SCI TECH (2018) 29:88
https://doi.org/10.1007/s41365-018-0415-z

Drop formation at nozzles submerged in quiescent continuous phase: an experimental study with TBP-dodecane and nitric acid system

Amitava Roy[1] · Mayur Darekar[2] · K. K. Singh[1,2] · K. T. Shenoy[2] · R. B. Grover[1]

Received: 28 July 2017 / Revised: 16 October 2017 / Accepted: 27 November 2017 / Published online: 4 May 2018

Abstract Solvent extraction is an important process in the nuclear fuel cycle. Tributyl phosphate (TBP) diluted with dodecane is commonly used as a solvent for extracting heavy metals from nitric acid medium. Studies on hydrodynamics of a single drop, which is the smallest mass transfer entity, are required for better understanding of the complex mass transfer and phase separation phenomena that occur in extraction equipment. In this study, drop formation at nozzles is studied using 30% TBP-dodecane as the dispersed phase and dilute nitric acid as the quiescent continuous phase. Experiments are carried out to determine the drop diameter, jetting velocity, drop detachment height and drop detachment time for various dispersed phase velocities, nozzle diameters (1.91, 3.04, and 4.88 mm), and nitric acid concentrations (0.01, 1, 3 N). Drop formation is captured using high-speed imaging, which enables quantification of drop size, onset of jetting, drop detachment height, and drop detachment time. Experimental data are used to propose correlations for predicting drop diameter and minimum jetting velocity. The correlations are found to be very accurate with average absolute relative errors being 5.23 and 2.97%, respectively.

Keywords Drop diameter · Drop detachment height · Drop detachment time · Jetting velocity · Solvent extraction · TBP-dodecane

List of symbols

C_D	Drag coefficient, -
d	Drop diameter, mm
d_N	Nozzle diameter, mm
g	Gravitational acceleration, m/s^2
L	Drop detachment height, mm
Q	Volumetric flow rate of dispersed phase through nozzle, mL/min
T	Drop detachment time, ms
U_j	Jetting velocity, m/s
U_N	Velocity through nozzle, m/s
V_{AN}	Volume of the drop attached to the nozzle, m^3

Greek letters

γ	Interfacial tension, N/m
ρ	Density, kg/m^3
$\Delta\rho$	Density difference, kg/m^3
μ	Viscosity, Pa.s

Subscript

c	Continuous phase
d	Dispersed phase

Dimensionless numbers

Eo	Eötvös number Eo = $g\Delta\rho d^2/\gamma$
Fr	Froude number Fr = U_N^2/gd_N

✉ Amitava Roy
amitava05roy@yahoo.co.in

✉ K. K. Singh
kksingh@barc.gov.in

[1] Homi Bhabha National Institute, Anushaktinagar, Mumbai 400094, India

[2] Chemical Engineering Division, Bhabha Atomic Research Centre, Mumbai 400085, India

1 Introduction

Solvent extraction is one of the most common separation processes used in the nuclear industry [1, 2]. Tributyl phosphate (TBP) diluted with dodecane is widely used as a solvent in the nuclear fuel cycle [3–5]. TBP is a preferred solvent due to its excellent chemical resistance, very low vapor pressure, and favorable physical properties. For example, the PUREX process uses 30% (v/v) TBP diluted with dodecane as a solvent due to its favorable chemistry for selective extraction of uranium (U) and plutonium (Pu), as well as splitting of Pu from U followed by stripping of U [6]. It is also used for extraction of other metal ions relevant to the nuclear fuel cycle [7]. Solvent extraction involves the transfer of a species from a dispersed liquid phase to a continuous liquid phase or vice versa through a liquid–liquid interface. The mass transfer rate depends on the mass transfer coefficient, interfacial area, concentration gradient, and important interfacial phenomena, such as flow conditions in the vicinity of interface and Marangoni convection. The diameter of the drop is one of the most important parameters as it controls the specific interfacial area and the diffusion–convection process, which are central to mass transfer [8]. The drop formation mechanism depends on the type of the equipment used. For example, in a mixer–settler, drops form due to turbulent eddies generated by a rotating impeller [9, 10], whereas in a centrifugal extractor or in a Taylor–Couette extractor, the drops form due to shearing between a rotating inner cylinder and a stationary outer cylinder [11–14]. In air pulsed columns, which are widely used for solvent extraction in the nuclear fuel cycle, drop formation occurs when the dispersed phase is pushed through perforations in sieve plates or through disc and doughnut type internals under the effect of pneumatic pulsing [15–18]. However, a prerequisite for understanding the drop formation phenomenon for such complex cases is a fundamental understanding of drop formation phenomenon for simple flow conditions. The present study focuses on drop formation at the tips of nozzles submerged in a quiescent immiscible liquid phase. It is a step in the direction of understanding drop formation phenomena in complex flow conditions, predictive model design, and simulation of solvent extraction equipment in the nuclear fuel cycle. Many more steps are required to reach the final goal. These steps include studying drop formation for different flow conditions such as in pulsating flow, counter-current flow, etc. We intend to study these cases in the future.

Drop diameter primarily depends on the geometry of the perforation (nozzle or orifice), the velocity of dispersed phase, interfacial tension, viscosity ratio, and the density difference between the two liquid phases. Harkins and Brown calculated the drop volume at very low flow rates by equating the buoyancy and interfacial tension forces and incorporating a correction factor to account for the drop volume that remains attached to the nozzle at the time of break-off [19]. The Harkins-Brown correction factor is empirical in nature [19, 20]. Hayworth and Treybal [21] as well as Null and Johnson [22] extended the work of Harkins and Brown. They proposed models that take into account the velocity effect and incorporate drag and inertial forces into the force balance equation. Scheele and Meister, Meister and Scheele, and Hamad and co-workers proposed a two-stage drop formation mechanism in which the drop formation process is divided into two stages, that is, drop growth during the first stage and necking, followed by drop detachment in the second stage [23–27]. In addition to the above-mentioned studies, numerical investigations have also been reported to study the hydrodynamics of single drop formation in laminar flow regime [28, 29]. Drop formation phenomenon depends significantly on the physical properties of the two liquids used. Though there are several studies on drop formation at nozzles, studies on drop formation for TBP diluted in dodecane–nitric acid system are scarce. This study aims to fill this gap.

In this work, experiments were carried out to determine the drop diameter, necking/jetting length, and drop detachment time as a function of the dispersed phase velocity at nozzles of different diameters and for different nitric acid concentrations. Variations in the nitric acid concentration cause variations in the physical and interfacial properties. High-speed imaging was used to capture the phenomenon of drop formation. The data obtained by carrying out image analysis were regressed to obtain correlations of drop diameter and minimum jetting velocity.

2 Experimental setup and procedure

A schematic diagram of the experimental setup is shown in Fig. 1. The experimental setup was made of borosilicate glass and stainless steel to avoid interfacial contamination. De-ionized water and commercial grade TBP, dodecane, and nitric acid were used. While the dispersed phase was always 30% (v/v) TBP in dodecane, nitric acid of three different concentrations (0.01, 1, and 3 N) was used as the aqueous phase. The organic (dispersed) and aqueous (continuous) phases were mutually saturated prior to experiments. Density, viscosity, and interfacial tension were experimentally determined using mutually saturated phases. The use of mutually saturated phases helped eliminate the effect of mass transfer on drop formation. The glass column was filled with the continuous phase. 30% (v/v) TBP in dodecane was pumped through the nozzle at the desired flow rate using a precision syringe

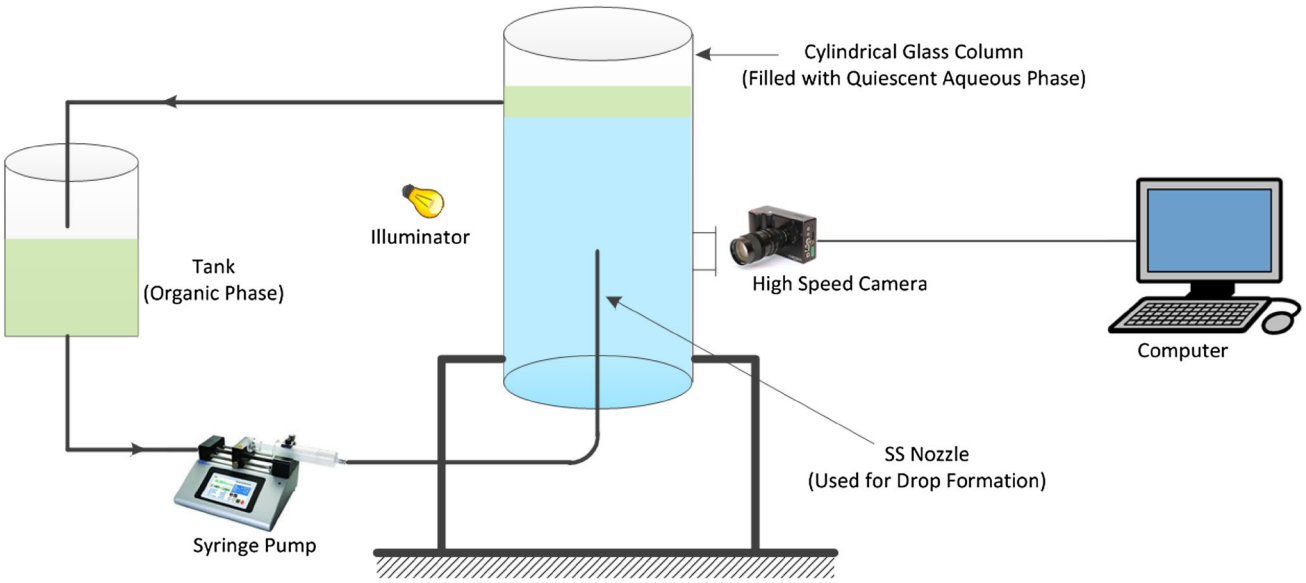

Fig. 1 (Color online) Schematic diagram of the experimental setup

pump, and drops were generated at the tip of the nozzle. The nozzle was observed on a computer screen in real time using a high-speed camera. The camera was set to capture video at a frame rate of 100–200 fps. The images acquired by the high-speed imaging system were stored on a PC as video clips. These clips were analyzed using ImageJ, which is a powerful image processing software tool. The time of formation of 10 drops was determined from video playback. From the knowledge of the volumetric flow rate of the dispersed phase as measured by the precision syringe pump, and the time of formation of 10 drops, the average volume of one drop and its equivalent diameter were calculated. The nozzle tip was in the field of view in each video. The image scale in terms of pixel per mm was obtained from the nozzle outer diameter. This scale was then used to measure the drop detachment height, i.e., the necking length and the jetting length. The drop formation time could be easily calculated from the recording speed (frames per second) and number of frames captured between the detachment of two successive drops.

The drop formation phenomenon at the tip of the nozzle submerged in a quiescent continuous phase depends on the nozzle diameter, dispersed phase velocity, and physical properties of the liquids. Thus, experiments were devised so that effects of these three variables on the drop formation phenomenon could be studied. To understand the effect of nozzle size, three different stainless steel nozzles were used in these experiments. The inner diameters (ID) of the nozzles were 1.91, 3.04, and 4.88 mm. For each nozzle, the experiments were conducted with nitric acid of three different concentrations (0.01, 1, and 3 N) as the aqueous phase so that the effects of physical properties could be studied. For each combination of nozzle diameter and nitric acid concentration, the flow rate of the dispersed phase was varied in the range of 4–40 mL/min in order to understand the effect of dispersed phase velocity. Thus, 88 experiments were conducted in total.

The physical and interfacial properties of mutually saturated test systems used in the experiments are presented in Table 1.

3 Results and discussion

The high-speed imaging system allowed visualization of drop formation phenomena, i.e., drop growth at the nozzle tip, onset of necking at intermediate values of velocity of the dispersed phase, and jet formation at higher velocities. The images acquired for the 1.91-mm-inner-diameter nozzle for phase system—I (see Table 1) are shown in Fig. 2. At lower velocities ($\leq$ 116 mm/s, or flow rate of $\leq$ 20 mL/min), the drop detachment point is very close to the nozzle tip, and the drop size is governed by the balance between buoyancy and interfacial tension forces. The onset of necking is observed at about 140 mm/s. The necking phenomenon observed in experiments agrees with that reported in the literature [28, 30]. Velocity effects in the form of inertial and drag forces contribute in the force balance equation as explained by Scheele and Meister [23, 24] and Hamad et al. [27].

Drop detachment height is measured from the tip of the nozzle. It is clearly observed from the captured images in Fig. 2 and later on from Fig. 4 that the increase in drop detachment height with increased velocity is gradual in the

Table 1 Physical properties (at 25° C) of the three mutually saturated phase systems used in the experiments

Test system		ρ (kg/m^3)	μ (cP)	$\Delta\rho$ (kg/m^3)	γ (mN/m)
Two-phase system—I					
Aqueous (c)	0.01 N nitric acid	1017	0.81	194	9.38
Organic (d)	TBP in dodecane[a]	823	1.54		
Two-phase system—II					
Aqueous (c)	1 N nitric acid	1032	0.83	208	9.62
Organic (d)	TBP in dodecane[a]	824	1.61		
Two-phase system—III					
Aqueous (c)	3 N nitric acid	1094	0.91	262	10.99
Organic (d)	TBP in dodecane[a]	832	1.70		

c continuous phase, *d* dispersed phase

[a]30%(v/v)TBP in dodecane

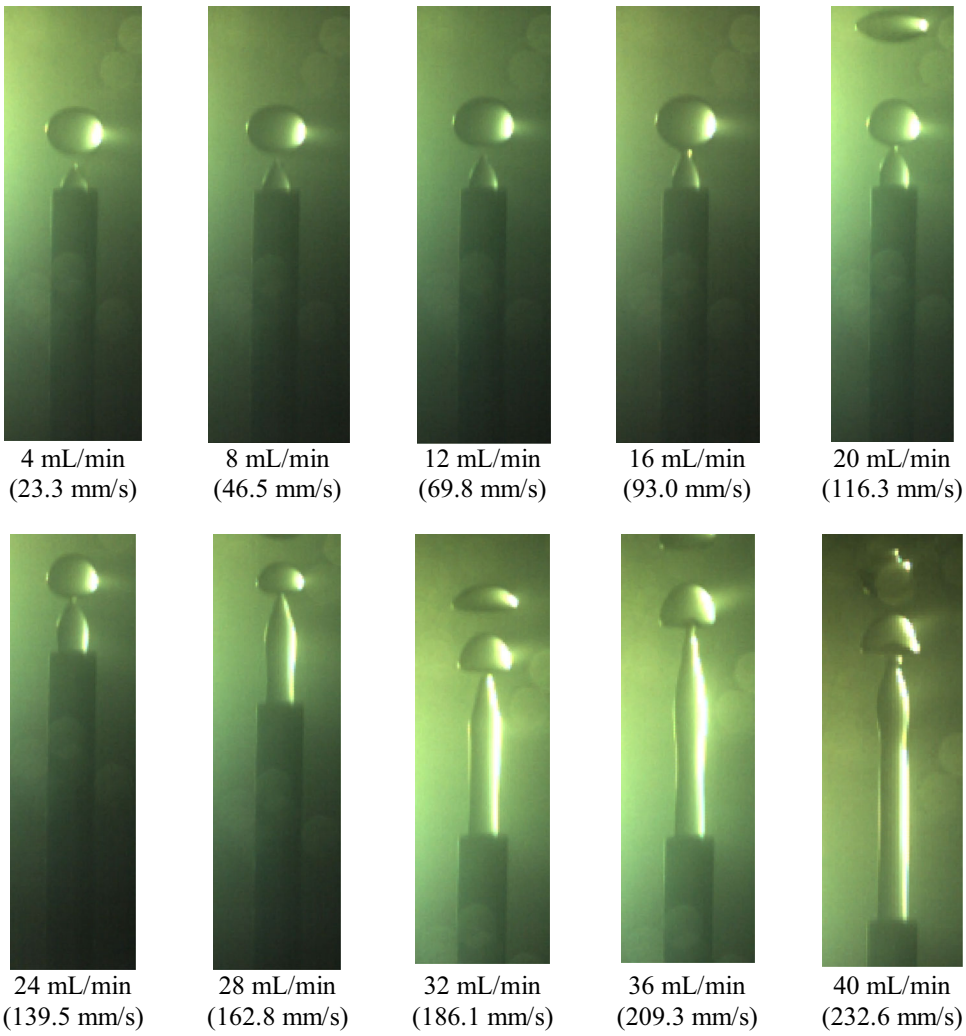

Fig. 2 (Color online) Images of drop formation at the tip of the 1.91-mm-inner-diameter nozzle for different dispersed phase flow rates (velocities). The images are for two-phase system—I {30% (v/v) TBP and dodecane − 0.01 N nitric acid}

necking regime and steep in the jetting regime. This is consistent with the observations of Scheele and Meister [23, 24], Meister and Scheele [25, 26], and Homma et al. [31]. A similar pattern was observed for the 3.04-mm-inner-diameter nozzle, whereas the jetting phenomena could not be captured due to the limited velocity range in the 4.88-mm-inner-diameter nozzle.

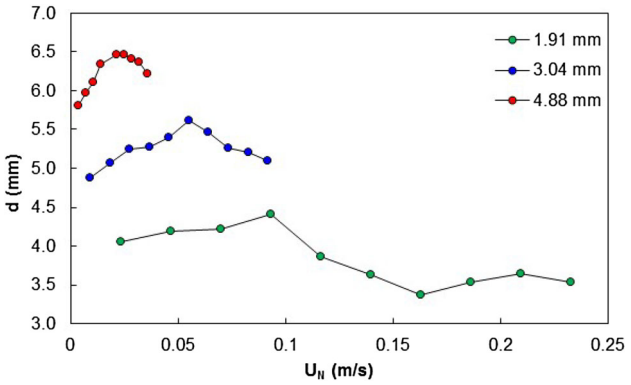

Fig. 3 (Color online) Effect of the dispersed phase velocity on drop diameter for the three nozzles used in experiments with two-phase system—I

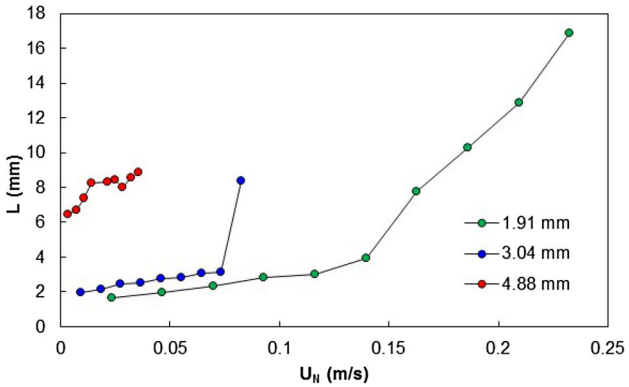

Fig. 4 (Color online) Effect of the dispersed phase velocity on drop detachment height for the three nozzles used in experiments with two-phase system—I

3.1 Effect of dispersed phase velocity and nozzle diameter

Figure 3 shows the dependence of drop diameter on the dispersed phase velocity through the nozzle. The drop diameter first increases up to a maximum value with increase in the dispersed phase velocity, then reduces with continued increase in the dispersed phase velocity. This trend is in agreement with the two-stage drop formation model proposed in the literature [23, 24, 32–34]. At a lower dispersed phase velocity, the drop size is governed by the balance between the buoyancy $\{V_{AN}\Delta\rho g\}$ and interfacial tension $\{\pi d_N\gamma\}$ forces. As the velocity increases, the kinetic $\{4/3\rho_d U_N Q\}$ and drag $\{C_D\mu Q(d_N/d)^n/d\}$ forces also contribute to the force balance equation. Among these forces, the interfacial tension force and drag force are the restraining forces, whereas the buoyancy force and the kinetic force are the lifting forces. The onset of necking is attributed to a larger lifting force. The dispersed phase continues to flow into the drop through the neck until the break-off time. Eventually, the diameter of the detached drop depends on the complex balance between the forces and the necking phenomenon. This complex force balance causes the drop diameter to first increase and then decrease with an increase in the dispersed phase velocity. Figure 3 shows that the drop diameter increases with an increase in the nozzle diameter. An increase in the interfacial force due to an increased nozzle diameter requires a higher lifting force, which is realized only with a larger drop. This causes drop diameter to increase with an increase in the nozzle diameter.

Figure 4 shows the effects of the dispersed phase velocity and nozzle diameter on the drop detachment height. It is observed that the drop detachment height first increases linearly but moderately with increased dispersed phase velocity as can be seen from the slope of the initial part of the curves in Fig. 4. Beyond a certain dispersed phase velocity, the drop detachment height increases steeply with increased dispersed phase velocity. This transition marks the transition from the necking to the jetting regime. The velocity at which this transition occurs is called the minimum jetting velocity. For the same velocity, the drop detachment height increases with an increase in nozzle diameter. The above observations are in agreement with the simulation results reported by Soleymani et al. [28]. Increased nozzle diameter results in thicker neck which takes a longer distance from the nozzle to thin out and break.

The drop detachment time, shown in Fig. 5, is the time between the detachment of two successive drops. Actually, it is the total of separation, spreading, growth, and necking/jetting period, as suggested by Soleymani et al. [28]. Drop detachment time depends strongly on the nozzle geometry, as well as the wettability of the materials. In the present case, there is no drop spreading as the stainless steel nozzle is not wetted by the organic phase. In the range of velocity covered in this study, the observed trend of drop detachment time is the same for all nozzles. As the velocity

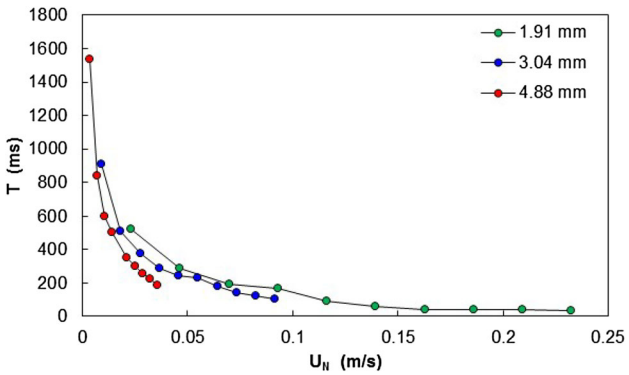

Fig. 5 (Color online) The effect of dispersed phase velocity on drop detachment time for the three nozzles used in experiments with two-phase system—I

increases, the time interval between detachment of two successive drops decreases. This is due to the increased kinetic force with increased dispersed phase velocity. An increased nozzle diameter results in reduced drop detachment time, which is in agreement with the observation of Soleymani et al. [28].

The experimental data were highly reproducible, as shown in Fig. 6. This figure depicts drop diameter variation with flow rate for two different experimental datasets. The error bars represent ± 5% of the values of the first experimental data set.

3.2 Effect of nitric acid concentration

The extraction and stripping chemistry of the TBP-dodecane solvent depends on the nitric acid concentration, which typically ranges from 0.01 to 3 N [14–16, 35]. The extraction of heavy metals is carried out at about 3N nitric acid concentration due to higher value of distribution coefficient at this concentration, whereas the stripping is carried out at 0.01 N nitric acid as the TBP–metal complex is unstable at lower concentrations. Physical properties of the aqueous phase change with nitric acid concentration. Thus, drop formation dynamics is also affected by nitric acid concentration. Therefore, it is necessary to study the effect of nitric acid concentration on drop diameter, drop detachment height, and drop detachment time. Figure 7 shows how the dispersed phase velocity affects the drop diameter for three different aqueous phases with different nitric acid concentrations. The trend of increase and subsequent decrease of drop diameter with increase in velocity is observed for all nitric acid concentrations and is in conformity with the two-stage drop formation model. For nitric acid concentrations ranging from 0.01 to 3 N, the interfacial tension increases marginally from 9.38 to 10.99 mN/m, whereas the density difference between the phases increases from 194 to 262 kg/m^3. Thus on increasing nitric acid concentration, an increased density difference is significant compared to the marginal increase in interfacial tension. Thus, with an increase in nitric acid concentration, the increase in the buoyancy force is more pronounced than the increase in the interfacial tension force. This causes the drop diameter to reduce with increasing nitric acid concentration.

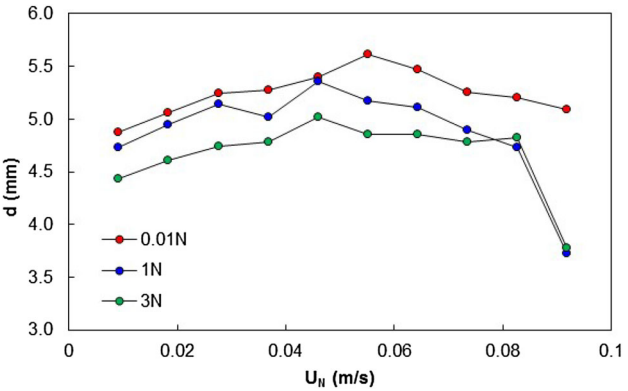

Fig. 7 (Color online) Effect of dispersed phase velocity on drop diameter for three nitric acid concentrations in the quiescent continuous phase (nozzle diameter = 1.91 mm)

Figure 8 shows the effect of dispersed phase velocity on the drop detachment height for three different nitric acid concentrations. As nitric acid concentration increases, the transition from necking to jetting occurs at a higher velocity. Higher jetting velocity at higher nitric acid concentration is attributed to higher values of interfacial tension. However, the effect is not significant for the range of interfacial tension values covered in this study. Figure 9 shows that for a given dispersed phase velocity, the drop detachment time is lower at higher nitric acid concentration. A lower drop detachment time at higher nitric acid concentration is attributed to higher value of density difference, leading to an increased buoyancy force and resulting in a faster detachment of drops.

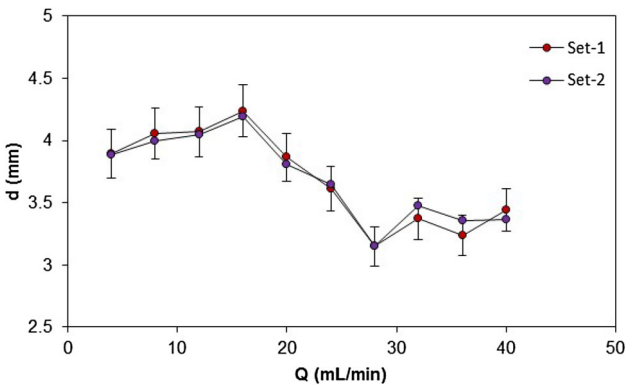

Fig. 6 (Color online) Reproducibility of the data showing drop diameter variation with dispersed phase flow rate for the 1.91-mm-ID nozzle used in experiments with two-phase system—II

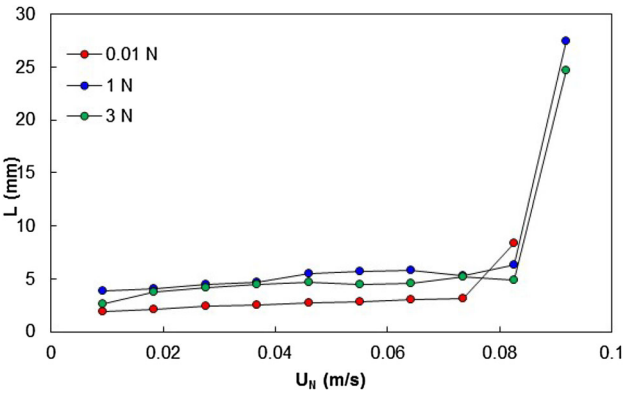

Fig. 8 (Color online) The effect of velocity on drop detachment height for three nitric acid concentrations in the quiescent continuous phase (nozzle diameter = 1.91 mm)

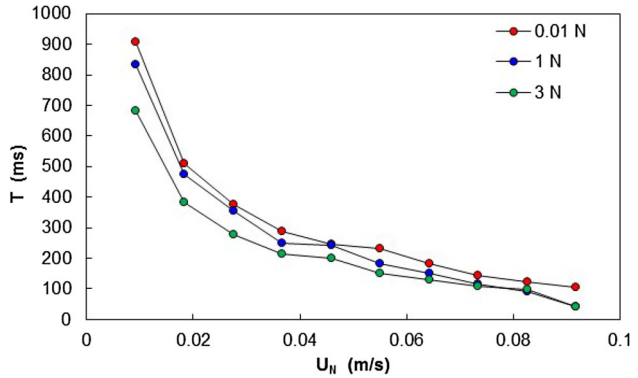

Fig. 9 (Color online) The effect of velocity on drop detachment time for three nitric acid concentrations in the quiescent continuous phase (nozzle diameter = 1.91 mm)

3.3 Correlation for drop diameter

Since drop diameter is a very important hydrodynamic variable which directly affects specific interfacial area for mass transfer, its accurate prediction is necessary for a given combination of independent variables, such as dispersed phase velocity and nozzle diameter. The experimental data obtained in this study were regressed to obtain correlations of drop diameter. The nonlinear regression was done by using Lab Fit curve fitting software [36]. When all the experimental data are used for regression, the drop diameter could be correlated by Eq. (1).

$$\frac{d}{d_N} = \frac{2.1962}{\mathrm{Eo}} + 0.76739\exp(-0.3976\mathrm{Fr}) - \frac{0.82523}{\mathrm{Eo}^2} \quad (1)$$

The average absolute relative error in the fit of Eq. (1) is 5.23%. The parity plot is shown in Fig. 10. Eo is the Eötvös number, which represents the ratio of buoyancy force to interfacial tension force. Fr is the Froude number, which represents the ratio of inertial force to the gravitational force. Eo and Fr are expressed by Eqs. (2) and (3), respectively. These dimensionless numbers account for all the restraining and lifting forces that affect the drop formation phenomenon.

$$\mathrm{Eo} = \frac{(\rho_c - \rho_d) g d_N^2}{\gamma} \quad (2)$$

$$\mathrm{Fr} = \frac{U_N^2}{g d_N} \quad (3)$$

If only experimental data prior to jetting are used, regression leads to the correlation given by Eq. (4). The average absolute relative error in the fit of Eq. (4) is 4.24% which is slightly better than the fit of Eq. (1). The parity plot of the correlation given by Eq. (4) is shown in Fig. 11.

$$\frac{d}{d_N} = 2.0347\mathrm{e}^{(0.0058342\mathrm{Eo} - 0.10727\mathrm{Fr}^2)} - 0.57065\ln(\mathrm{Eo}) \quad (4)$$

3.4 Correlation for minimum jetting velocity

The jetting velocity (U_j) is the minimum velocity of the dispersed phase through the nozzle at which the jet forms. It is important to know the minimum jetting velocity for a given phase system (physical properties) and nozzle diameter as it separates the necking and jetting regimes. In this work, we have tested two of the previously reported correlations for minimum jetting velocity and adapted them for use with our experimental data. The previously reported correlations of Ryan [37] and de Chazal and Ryan [33] were tested. These correlations are given by Eqs. (5) and (6), respectively.

$$U_j = 1.16\left(\frac{\gamma}{\Delta\rho g d_N^2}\right)^{0.95} (d_N g)^{0.5} \left(\frac{\Delta\rho}{\rho_d}\right) \quad (5)$$

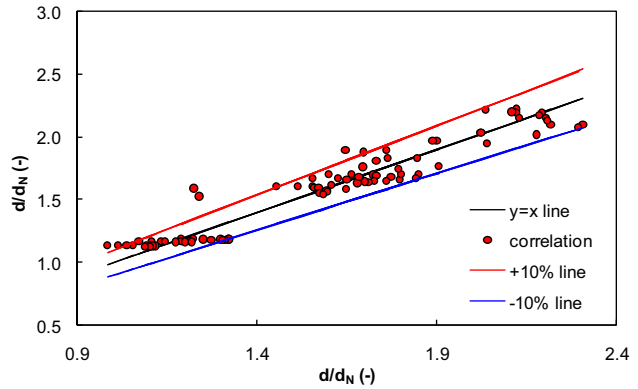

Fig. 10 (Color online) Parity plot of the experimental values of d/d_N and d/d_N values predicted by the correlation of Eq. (1) considering all experimental data

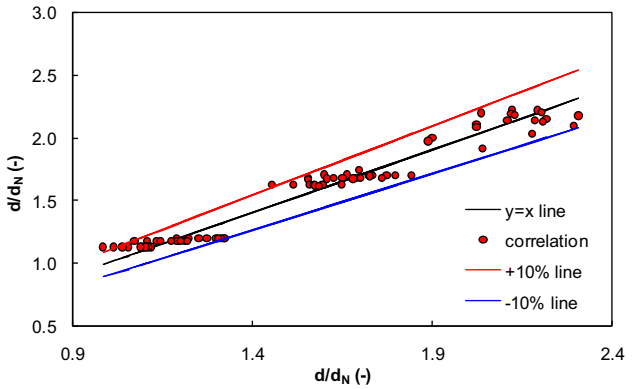

Fig. 11 (Color online) Parity plot of the experimental values of d/d_N and d/d_N values predicted by the correlation of Eq. (4) by considering experimental data of the dripping regime only

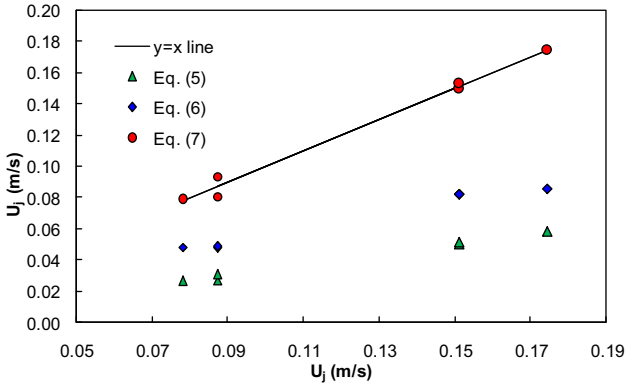

Fig. 12 (Color online) Parity plot of the experimental and predicted values of minimum jetting velocity

$$U_j = \sqrt{\frac{2\gamma}{\rho_d d_N}}\left(1.07 - 0.75\sqrt{\frac{\Delta\rho g d_N^2}{4\gamma}}\right) \tag{6}$$

The above correlations are tested with our limited experimental data (6 data points) for minimum jetting velocity. The correlation of Ryan is found to give an average absolute relative error of about 64%, whereas the correlation of de Chazal and Ryan is found to give an average absolute relative error of about 40%. Since the correlation of de Chazal and Ryan is found to give a better match, it is adapted to fit our experimental data. Due to the limited experimental data, we attempted a two parameter model with $\sqrt{2\gamma/\rho_d d_N}$ and $\sqrt{\Delta\rho g d_N^2/4\gamma}$ as the independent variables. The correlation given by Eq. (7) is obtained with a very low average absolute relative error of only 2.97%. Figure 12 shows the parity plot of the jetting velocity obtained experimentally with that predicted by Eqs. (5)–(7).

$$U_j = 13.8138\left(\frac{2\gamma}{\rho_d d_N}\right) - 0.0364321\sqrt{\frac{\Delta\rho g d_N^2}{4\gamma}} \tag{7}$$

4 Conclusion

Hydrodynamics of formation of a single drop of 30% (v/v) TBP-dodecane solvent in a quiescent dilute nitric acid phase is studied with varying dispersed phase velocity and using nozzles of different diameters. Nitric acid concentration is varied from 0.01 to 3 N. The drop formation process was captured by high-speed imaging, and various stages of drop formation, i.e., drop growth, necking, jetting, and drop detachment, are distinctly observed in the images. The drop diameter is found to first increase and subsequently decrease with increase in dispersed phase velocity. The effect of velocity on drop detachment height clearly indicates a transition from the necking to the jetting regime. The drop detachment time is found to reduce with an increase in dispersed phase velocity. For a given dispersed phase velocity, an increased nozzle diameter leads to an increased drop diameter and drop detachment height and a reduced drop detachment time. The drop diameter and drop detachment time are found to reduce with reduce in nitric acid concentration. The drop detachment height does not vary significantly with change in nitric acid concentration. The minimum jetting velocity is found to be higher for a smaller diameter nozzle. The minimum jetting velocity is found to be lower for a lower nitric acid concentration. Nonlinear regression is used to obtain the correlations for drop diameter and minimum jetting velocity. The resulting correlations are found to be very accurate with average absolute relative errors less than 6%. The proposed correlations will be useful for estimating drop size, as well as to quantify the onset of jetting in a two-phase system involving 30%(v/v) TBP-dodecane and nitric acid, which is widely used for liquid–liquid extraction-based separation processes in the nuclear fuel cycle.

Acknowledgements Amitava Roy gratefully acknowledges the support provided for conducting experiments by Chemical Engineering Group and the measurement of interfacial tension by Radiochemistry and Isotope Group of Bhabha Atomic Research Centre.

References

1. Y. Cui, X.F. Yang, C. Yang et al., Solvent extraction of U(VI) by N, N-dimethyl-N′, N′-dioctylsuccinylamide and N, N-dimethyl-N′, N′-didecylsuccinylamide in cyclohexane. Nucl. Sci. Tech. **27**, 59 (2016). https://doi.org/10.1007/s41365-016-0056-z
2. Z. Dong, W.J. Yuan, C. Liu et al., Th(IV) and U(VI) removal by TODGA in ionic liquids: extraction behavior and mechanism, and radiation effect. Nucl. Sci. Tech. **28**, 62 (2017). https://doi.org/10.1007/s41365-017-0214-y
3. A.P. Paiva, P. Malik, Recent advances on the chemistry of solvent extraction applied to the reprocessing of spent nuclear fuels and radioactive wastes. J. Radioanal. Nucl. Chem. **261**, 485–496 (2004). https://doi.org/10.1023/B:JRNC.0000034890.23325.b5
4. H. Hotokezaka, M. Tokeshi, M. Harada et al., System for high-level radioactive waste using microchannel chip - extraction behavior of metal ions from aqueous phase to organic phase in microchannel. Prog. Nucl. Energy **47**, 439–447 (2005). https://doi.org/10.1016/j.pnucene.2005.05.045
5. R. Natarajan, Reprocessing of spent nuclear fuel in India: Present challenges and future programme. Prog. Nucl. Energy **101**, 118–132 (2017). https://doi.org/10.1016/j.pnucene.2017.03.001
6. P. Vishnu Anand, R. Rajeev, P. Velavendan et al., Modeling and simulation of diluent recovery unit in PUREX solvent regeneration system. Prog. Nucl. Energy **104**, 359–367 (2017). https://doi.org/10.1016/j.pnucene.2017.01.011
7. S.R. Reddy, R. Trikha, R. Murali et al., Extraction kinetics of ruthenium in the mixture of tri-n-butyl phosphate and n-dodecane. Prog. Nucl. Energy **86**, 50–62 (2016). https://doi.org/10.1016/j.pnucene.2015.10.003
8. M. Wegener, N. Paul, M. Kraume, Fluid dynamics and mass transfer at single droplets in liquid–liquid systems. Int. J. Heat

Mass Transf. **71**, 475–495 (2014). https://doi.org/10.1016/j.ijheatmasstransfer.2013.12.024
9. A.O. de Santana, C.C. Dantas, Scale up of the mixer of a mixer-settler model used in a uranium solvent extraction process. J. Radioanal. Nucl. Chem. **189**, 257–269 (1995). https://doi.org/10.1007/BF02042604
10. K.K. Singh, S.M. Mahajani, K.T. Shenoy et al., Representative drop sizes and drop size distributions in A/O dispersions in continuous flow stirred tank. Hydrometallurgy **90**, 121–136 (2008). https://doi.org/10.1016/j.hydromet.2007.10.003
11. S. Kumar, D. Sivakumar, B. Kumar et al., Development of a miniature Taylor-Couette extractor column for nuclear solvent extraction. J. Radioanal. Nucl. Chem. **292**, 1237–1240 (2012). https://doi.org/10.1007/s10967-012-1688-z
12. M. Zhao, S. Cao, W. Duan, Effects of some parameters on mass-transfer efficiency of a ϕ20 mm annular centrifugal contactor for nuclear solvent extraction processes. Prog. Nucl. Energy **74**, 154–159 (2014). https://doi.org/10.1016/j.pnucene.2014.02.024
13. K. Mandal, S. Kumar, V. Vijayakumar et al., Hydrodynamic and mass transfer studies of 125 mm centrifugal extractor with 30% TBP/nitric acid system. Prog. Nucl. Energy **85**, 1–10 (2015)
14. S.V.N. Ayyappa, M. Balamurugan, S. Kumar et al., Mass transfer and hydrodynamic studies in a 50 mm diameter centrifugal extractor. Chem. Eng. Process. **105**, 30–37 (2016). https://doi.org/10.1016/j.pnucene.2015.05.005
15. J.Q. Liu, S.W. Li, S. Jing, Axial mixing and mass transfer performance of an annular pulsed disc-and-doughnut column. Solv. Extr. Ion Exch. **33**, 592–606 (2015). https://doi.org/10.1080/07366299.2015.1074453
16. N. Sen, K.K. Singh, A.W. Patwardhan et al., CFD Simulation of two-phase flow in pulsed sieve plate column—identification of a suitable drag model to predict dispersed phase holdup. Sep. Sci. Tech. **51**, 2790–2803 (2016). https://doi.org/10.1080/01496395.2016.1218895
17. S. Sarkar, N. Sen, K.K. Singh et al., Effect of operating and geometric parameters on dispersed phase holdup in pulsed disc and doughnut and pulsed sieve plate columns: a comparative study. Chem. Eng. Process. **118**, 131–142 (2017). https://doi.org/10.1016/j.cep.2017.04.016
18. P. Amani, J. Safdari, A. Gharib et al., Mass transfer studies in a horizontal pulsed sieve-plate column for uranium extraction by tri-n-octylamine using axial dispersion model. Prog. Nucl. Energy **98**, 71–84 (2017). https://doi.org/10.1016/j.pnucene.2017.02.010
19. W.D. Harkins, F.E. Brown, The determination of surface tension (free surface energy) and the weight of falling drops—surface tension of water and benzene by the capillary height method. J. Am. Chem. Soc. **41**, 499 (1919). https://doi.org/10.1021/ja01461a003
20. Y.H. Mori, Harkins–Brown correction factor for drop formation. AIChE J. **36**, 1272–1274 (1990). https://doi.org/10.1002/aic.690360819
21. C.B. Hayworth, R.E. Treybal, Drop formation in two liquid phase systems. Ind. Eng. Chem. **42**, 1174–1181 (1950). https://doi.org/10.1021/ie50486a030
22. H.R. Null, H.F. Johnson, Drop formation in liquid–liquid systems from single nozzles. AIChE J. **4**, 273–281 (1958). https://doi.org/10.1002/aic.690040308
23. G.F. Scheele, B.J. Meister, Drop formation at low velocities in liquid–liquid systems. Part I. Prediction of drop volume. AIChE J. **14**, 9–15 (1968). https://doi.org/10.1002/aic.690140105
24. G.F. Scheele, B.J. Meister, Drop formation at low velocities in liquid–liquid systems: part II. Prediction of jetting velocity. AIChE J. **14**, 15–19 (1968). https://doi.org/10.1002/aic.690140106
25. B.J. Meister, G.F. Scheele, Prediction of jet length in immiscible liquid systems. AIChE J. **15**, 689–699 (1969). https://doi.org/10.1002/aic.690150512
26. B.J. Meister, G.F. Scheele, Drop formation from cylindrical jets in immiscible liquid systems. AIChE J. **15**, 700–706 (1969). https://doi.org/10.1002/aic.690150513
27. F.A. Hamad, M.K. Khan et al., Comparison of experimental results and numerical predictions of drop diameter from a single submerged nozzle in a liquid–liquid system. Can. J. Chem. Eng. **79**, 322–328 (2001). https://doi.org/10.1002/cjce.5450790304
28. A. Soleymani, A. Laari, I. Turunen, Simulation of drop formation in a single hole in solvent extraction using the volume-of-fluid method. Chem. Eng. Res. Des. **86**, 731–738 (2008). https://doi.org/10.1016/j.cherd.2008.03.024
29. Y. Chen, L. Wu, C. Zhang, Emulsion droplet formation in coflowing liquid streams. Phys. Rev. E **87**, 013002 (2013). https://doi.org/10.1103/PhysRevE.87.013002
30. A. Kumar, S. Hartland, Prediction of drop size produced by a multiorifice distributor. Trans. Inst. Chem. Eng. **60**, 35–39 (1982)
31. S. Homma, J. Koga, S. Matsumoto et al., Breakup mode of an axisymmetric liquid jet injected into another immiscible liquid. Chem. Eng. Sci. **61**, 3986–3996 (2006). https://doi.org/10.1016/j.ces.2006.01.029
32. E.V.L.N. Rao, R. Kumar, N.R. Kuloor, Drop formation studies in liquid–liquid systems. Chem. Eng. Sci. **21**, 867–880 (1966). https://doi.org/10.1016/0009-2509(66)85081-9
33. L.E.M. de Chazal, J.T. Ryan, Formation of organic drops in water. AIChE J. **17**, 1226–1229 (1971). https://doi.org/10.1002/aic.690170531
34. N.W. Geary, R.G. Rice, Bubble size prediction for rigid and flexible spargers. AIChE J. **37**, 161–168 (1991). https://doi.org/10.1002/aic.690370202
35. N. Sen, M. Darekar, K.K. Singh et al., Solvent extraction and stripping studies in microchannels with TBP nitric acid system. Sol. Extr. Ion Exch. **32**, 281–300 (2014). https://doi.org/10.1080/07366299.2013.850290
36. W.P. Da Silva, C.M.D.P.S. Cavalcanti, C.G.B. Silva et al., LAB fit curve fitting: a software in portuguese for treatment of experimental data. Rev. Bras. Ensino. Fis. **26**, 419–427 (2004). https://doi.org/10.1590/s1806-11172004000400018
37. J.T. Ryan, Ph.D. thesis, University of Missouri, (1966)